doi:10.1038/nature12567

Supplementary Discussion

1. Biases in previous icebergs estimates

Iceberg distributions from ship-based observations are spatially and temporally limited to a small fraction of the Southern Ocean and to the Austral summer when a peak in iceberg concentration has been detected from satellite[32]. Gladstone and Bigg[33] also point out that shipping routes are mostly near the coast where iceberg concentration is high, and that there is an observer positive bias on the number of icebergs sighted. Converting iceberg concentration to calving flux also requires certain assumptions regarding the "life expectancy" of icebergs[2]. We expect most of the errors in previous estimates to come from estimation of small icebergs (half the estimated calving flux[1]) as they are reliant on ship borne observations, while large icebergs can be tracked from satellite. Errors on volume are also likely to be smaller for larger icebergs.

2. Ice thickness from surface elevation

Ice thickness derived from surface elevation is critical for determining the CF for all ice shelves, for estimating GLF for the 32% of the flux where ice penetrating radar data were not available and, therefore, by definition for BMB. Accurate and reliable surface elevations and their conversion to thickness is, therefore, a critical step in the analysis.

Importantly, we did not use a derivative ice thickness product such as BEDMAP2[34] as was done in another study of bottom melt rates from mass continuity[35], or the original thickness at the grounding line from Griggs and Bamber[19]. We did not use the former because it is a merged combination of Griggs and Bamber and interpolated grounded ice thickness estimates aimed at providing continuity at the grounding line, but not necessarily to be consistent with the original data. We did not use the latter because the interpolation of the surface elevation data is sensitive to the location of the grounding line[19,36] and because we needed to apply a correction for elevation change (dh/dt) between 1995 and 2009, and a new firn air content correction to the surface elevations *before* converting to thickness. These corrections are significant and represent an important difference with another recent study of basal melt rates[35]. A 10 cm yr^{-1} dh/dt, for example, would result in about a 14 m difference in estimated thickness, which represents as much as a 10% difference in CF. During the ICESat period from 2003-2009, rates exceeding 25 cm yr^{-1} were observed over several shelves[8]. Firn air content was determined from the regional climate model RACMO2[31] in a similar approach to Griggs and Bamber (19) but with the model running at half the resolution (27.5 km vs 55 km). The improvement in resolution has a significant impact on the spatial pattern of the firn air content correction, given the size of many ice shelves. Our thicknesses at the grounding line (and elsewhere) are therefore an improvement on previously published data[19], and unique to this study.

3. Interpolation of un-surveyed sectors

Our calving/melting analysis covers 90% of the ice sheet area and 76% of its surface mass balance. The analysis was not possible for the smallest ice shelves, less than about 100 km^2, which form on the coast of slow moving ice in between fast flowing ice streams and outlet glaciers (Supplementary Figure 6). These shelves lie below the detection threshold of satellite altimetry and therefore we are unable to obtain their ice thickness. In order to account for these un-surveyed areas, we make the assumption (supported by the results of both radar and laser altimetry[9,30]) that the areas are close to balance and therefore, the GLF is close to the drainage

basin surface mass balance. We include a 10% deviation from balance in our uncertainty estimate for the interpolated GLF, in addition to the uncertainty in surface mass balance. We chose reference ice shelves by comparing the oceanographic setting (warm/cold water)[8] and melt ratios and excluded the four largest ice shelves (FRIS, RIS, AIS, and LBC) as their interaction with the ocean is not characteristic of the smallest ice shelves. For the areas in sector I''- B, we use BRL, JF, AR and NE (Supplementary Figure 1 and 6). For the sector C-F', we use all ice shelves of that sector except RIS, TOT and MU. All ice shelves of sector F'-I' are used for the un-surveyed areas within this sector. The uncertainty in partitioning the flux between BMB and CF is determined from the standard deviation of the melt ratio (MR) for the reference area ice shelves.

4. Comparison with previous basal melt estimates

Various studies have used different approaches to estimate the melt rate beneath ice shelves. They have, in general, focused on a handful of ice shelves. Comparison with previous studies using similar methods shows, in general, reasonable agreement[5,14,37]. The differences that remain with Yu et al.[14] for the AIS (0.44 vs. 0.65 ± 0.35 m yr^{-1} in this study) are a consequence of the difference in GLF as our CF and SMB are very similar. However, Wen et al.[37] obtain results close to ours (0.76 m yr^{-1}). The difference between our results and those of Joughin and Padman[5] for the FRIS (0.2 vs. 0.12 ± 0.09 m yr^{-1}, here) is due to the use of a suite of different data sets for i) SMB, ii) GLF, iii) geoid correction, iv) firn air content correction and v) correcting for non-steady state. Our results agree fairly well with those of Potter et al.[23] for George VI ice shelf (2.0 vs. 2.88 ± 0.32 m yr^{-1}). It is less easy to compare with specific BMB, i.e. point measurements or flow line flux divergence estimates. For the FRIS, these range from 0.18-0.55 m yr^{-1} but do not generally incorporate the central, high accretion part of the Ronne ice shelf[15]. Our estimate lies at the lower end of oceanic studies[38,39] that obtained mean specific basal mass balance (SBMB) of 0.10-0.20 m yr^{-1} for a complete ice front oceanic survey.

5. Grounding line and ice shelf mask

The only complete ice shelf grounding lines for the Antarctic ice sheet are the products of the MODIS Mosaic of Antarctica (MOA)[40] and the Antarctic Surface Accumulation and Ice Discharge (ASAID) project[41]. These groundling lines are derived from the break in slope that can be observed in optical satellite imagery in the transition zone between grounded ice and free-floating ice, also known as the grounding zone. The boundaries of this zone can further be mapped using repeated ICESat altimetry[42] or differential InSAR[43] by investigating the flexure limits of the vertical fluctuations induced by ocean tides. The three techniques produce relatively consistent grounding lines in stagnant and slow-moving areas, but over fast-moving ice streams the break in slope can be hard to detect and may sometimes deviate by tens of kilometres from the landward flexure limit[43]. In this study, we estimate mass fluxes at the point where ice leaves the ground, so therefore we prioritize InSAR and ICESat data where available. The next paragraphs describe how we compile and optimize grounding line and ice shelf mask for the whole of Antarctica based on the newest and most suitable datasets.

We started with the point dataset of the ASAID grounding line[41] which we converted into a polygon and merged with the more complete ice rises and islands of MOA 2003-04 [40]. We smoothed and simplified the polygons to within an accuracy of 50 m to reduce the number of vertices. The resulting grounding-line polygons were then adjusted manually to fit within 1 km of the discontinuous grounding data from InSAR[43] and ICESat[44,45]. We selected the newest and most continuous data whenever multiple InSAR/ICESat grounding lines were available. ICESat points were only used when the coverage was sufficient to determine a continuous line.

We also made some local adjustments in accordance with more recent studies on grounding line dynamics:

- Pine Island Glacier; updated with InSAR data from 2009([46])
- Thwaites Glacier; replaced with IceBridge data from 2009([47])
- Thwaites Ice Tongue; ice rises added and removed[47,48]
- Smith Glacier; updated with MODIS data from 2007([49])
- Amery Ice Shelf; complemented with InSAR and MODIS data[50]
- Beaver Lake; included as a part of the Amery Ice Shelf[51]
- Evans Ice Stream; complemented with additional InSAR data[52]
- Larsen C Ice Shelf; updated with the Bawden Ice Rise[53]

We generated ice shelf outlines by intersecting the grounding-line polygons with the MOA 2003-04 coastline. We removed all resulting polygons that were smaller than 1 km^2 or that did not look like ice shelves in the image mosaics of MOA, RAMP[54] and LIMA[55]. The resulting ice shelf mask contains 238 ice shelves with a total area of 1,554,800 km^2. Islands and ice rises within ice shelves represent 191,694 km^2. This complete ice shelf mask is cropped with the coverage of our ice shelf thickness and both figures become 1,481,063 km^2 and 113,041 km^2, respectively.

6. Calving flux sensitivity to gate placement

Steady state calving fluxes (CFs) are best approximated by ice velocity and thickness observations close to the calving front. By doing so, calving events occurring on a decadal to multi-decadal time scale are averaged to annual fluxes. However, if the measurement is taken before/after a calving event (within a calving cycle), the thickness is expected to be smaller/larger because of the higher bottom melt at the front[5]. Placing CF gates with increments of 10 km inland of our calving front gates (Supplementary Figure 2), we find that the maximum CF estimate of most ice shelves is obtained within 0-20 km of the ice front with small relative difference. The maximum total CF is found 10 km inland of our calving front gates and represents a 3% increase compared to our gates. The maximum CF can be 30 km inland (RIS, AR, SHA), 40 km (ADE, DRY), but not more than 50 km (FRIS, REN). The sum of each individual maximum represents an 8% increase (or ~100 Gt yr^{-1}). Irrespective of any thickness change due to dynamic thinning, this maximum CF means that the specific SMB (0.13-1.37 m yr^{-1}) is smaller in magnitude than the specific BMB. This limit is also an indication of how far inland the strong frontal melt from tidal and wind-induced mixing can reach. Our calving front gates are 2-10 km away from the actual calving front. Therefore our CFs are missing 2-10 km of bottom melt as well as the frontal underwater face melt[56]. To account for these two processes, and for the maximum flux (0-50 km inland) we add a 3% uncertainty to our calving flux estimates.

7. SMB uncertainty

The uncertainty in modelled specific SMB is derived from a comparison with 315 local specific SMB observations on Antarctic ice shelves[57]. These observations are mainly located on the larger Ross and Filchner-Ronne, although some are available on the smaller East Antarctic ice shelves as well (Supplementary Figure 3). The agreement between modelled and observed specific SMB is good (R=0.68), and the slope of the least-squares linear fit equals 1.0 indicating that there is no significant under- or over-estimation by RACMO2 (Supplementary Figure 4). For each of the observations, the observed and modelled specific SMB are compared, and the total uncertainty at each location is assumed to be the absolute difference between these two. This uncertainty can be ascribed to both an uncertainty in the observation

and in the model. For the uncertainty in the observations, we use a function that relates the uncertainty to the specific SMB itself in a linear fashion[58]. The remaining uncertainty, ascribed to the model, is calculated as the square root of the difference between the quadratic total uncertainty and the quadratic observational uncertainty. The resulting 315 model uncertainties are averaged to get a mean error of 38.0 mm yr^{-1} with a mean modelled specific SMB at the locations of the observations of 136.6 mm yr^{-1}. The relative uncertainty for the specific SMB on Antarctic ice shelves therefore equals 28%.

8. Firn correction uncertainty

The uncertainty in the total firn air content is calculated using a combination of the uncertainties in the three fixed points in the density profile of a steady state firn layer: i) the density at the surface (rho_0), ii) the depth of the 550 kg m^{-3} level (z_{550}) and iii) the depth of the 830 kg m^{-3} level (z_{830}). In the firn densification model (FDM)[31], rho_0 is calculated using a linear relation of near-surface temperature, average accumulation and 10 meter wind speed[59]. On Antarctica, rho_0 ranges between 300-470 kg m^{-3} and is assumed constant in time. The uncertainty in rho_0 is assumed to be 50 kg m^{-3}. The FDM is calibrated using observed z_{550} and z_{830} of ice cores. For both quantities the uncertainty is assumed to equal the averaged uncertainty in the observations: 1.9 m (z_{550}) and 2.7 m (z_{830}) (Figure 4 of Van den Broeke[60]). Supplementary Figure 5 shows the vertically integrated firn air content. The control density profile (black line) has a total firn air content of 14.0 m. The influence of the uncertainty in rho_0 is smallest, yielding a ~0.25 m uncertainty in total firn air content. For z_{550} and z_{830}, this is ~0.5 m. Combining the uncertainties gives a range of -1.52 m and +1.61 m around the control value. Therefore, we consider ~10% as a reasonable measure for the uncertainty in the firn air content as simulated by the FDM.

Supplementary Figures and Tables

Supplementary Table 1 Mass balance of observed Antarctic ice shelves.

Sector	Ice shelf	GLF	SMB	CF	dh/dt	BMB	Area	Area+	SBMB	MR	GLF Thick
		Gt yr^{-1}	Gt yr^{-1}	Gt yr^{-1}	Gt yr^{-1}	Gt yr^{-1}	10^3 km^2	10^3 km^2	m yr^{-1}	%	
AA'	AR	59 ± 14	25 ± 7	44 ± 5	-	-39 ± 16	88	90	-0.44 ± 0.18	47	HE-thick
A'B	NE	57 ± 15	8 ± 2	30 ± 7	-	-36 ± 16	10	10	-3.58 ± 1.63	54	HE-thick
BC	AIS	80 ± 20	9 ± 3	50 ± 6	-	-39 ± 21	60	60	-0.65 ± 0.35	44	HE-thick
CC'	W*	39 ± 9	7 ± 2	31 ± 4	-11 ± 8	-26 ± 13	16	16	-1.65 ± 0.82	46	HE-thick
AC' Upscaling		89 ± 10	-	49 ± 7	-	-40 ± 6	-	-		45	-
West Indian Ocean		235 ± 30	49 ± 8	155 ± 22	-11 ± 8	-140 ± 38	174	177	-0.80 ± 0.22	47	-
West Indian Ocean+		324 ± 31	-	204 ± 29	-11 ± 8	-179 ± 43	-	-	-	47	-
CC'	SHA*	48 ± 9	21 ± 6	34 ± 7	-41 ± 20	-76 ± 23	35	35	-2.20 ± 0.67	69	HE-thick
C'D	VAN	13 ± 3	1 ± 0	9 ± 3	-	-5 ± 4	1	1	-3.94 ± 3.73	33	HE-thick
C'D	TOT*	81 ± 9	8 ± 2	28 ± 8	-2 ± 2	-64 ± 12	6	6	-9.89 ± 1.92	70	IPR
C'D	MU	47 ± 6	4 ± 1	23 ± 5	-	-28 ± 7	6	6	-4.93 ± 1.32	55	IPR
C'D	POR*	47 ± 5	3 ± 1	36 ± 9	-3 ± 1	-18 ± 10	2	2	-8.09 ± 4.68	33	IPR
DD'	ADE*	16 ± 2	2 ± 1	7 ± 3	-3 ± 1	-13 ± 4	2	2	-8.40 ± 2.32	64	IPR
DD'	MER	20 ± 4	5 ± 1	20 ± 1	-	-5 ± 4	6	6	-0.87 ± 0.79	19	IPR
DD'	NIN	22 ± 2	1 ± 0	23 ± 2	-	0 ± 3	2	2	-0.16 ± 2.28	1	IPR
DD'	COO	33 ± 3	2 ± 1	32 ± 6	-	-3 ± 7	3	3	-0.92 ± 2.08	8	IPR
D'D	REN*	5 ± 2	1 ± 0	1 ± 0	-2 ± 1	-7 ± 2	3	3	-2.20 ± 0.58	90	HE-thick
C'D' Upscaling		175 ± 21	-	93 ± 31	-	-82 ± 27	-	-	-	47	-
East Indian Ocean		333 ± 16	48 ± 7	213 ± 44	-51 ± 20	-219 ± 48	65	66	-3.35 ± 0.73	51	-
East Indian Ocean+		508 ± 26	-	306 ± 75	-51 ± 20	-300 ± 80	-	-	-	50	-
D'E	DRY	8 ± 1	0 ± 0	3 ± 0	-	-5 ± 1	3	3	-1.88 ± 0.46	59	HE-thick
EF'	RIS	120 ± 15	61 ± 17	147 ± 9	-	-34 ± 25	477	484	-0.07 ± 0.05	19	IPR
EF'	SUL	21 ± 5	10 ± 3	3 ± 1	-	-28 ± 6	13	15	-2.16 ± 0.44	91	HE-thick
D'F' Upscaling		27 ± 3	-	14 ± 5	-	-12 ± 4	-	-	-	47	-
Ross Sea		149 ± 16	71 ± 17	153 ± 10	-	-67 ± 26	492	501	-0.14 ± 0.05	30	-
Ross Sea+		175 ± 16	-	167 ± 15	-	-79 ± 28	-	-	-	32	-
F'G	LAN*	16 ± 3	1 ± 0	11 ± 5	-1 ± 0	-6 ± 6	1	1	-9.79 ± 9.81	35	HE-thick
F'G	GET*	92 ± 10	36 ± 10	56 ± 14	-63 ± 12	-136 ± 23	33	34	-4.09 ± 0.68	71	IPR
GH	CD*	51 ± 5	9 ± 2	18 ± 2	-36 ± 3	-78 ± 7	8	8	-9.47 ± 0.83	81	IPR
GH	THW*	102 ± 10	4 ± 1	62 ± 14	-26 ± 2	-69 ± 18	5	5	-15.22 ± 3.87	53	IPR
GH	PI*	110 ± 11	4 ± 1	50 ± 8	-30 ± 2	-95 ± 14	6	6	-15.96 ± 2.38	65	IPR
GH	COS	11 ± 3	2 ± 0	2 ± 0	-	-11 ± 3	3	3	-3.74 ± 0.89	88	HE-thick
F'H Upscaling		123 ± 14	-	34 ± 7	-	-89 ± 20	-	-	-	72	-
Amundsen Sea		383 ± 19	55 ± 11	198 ± 43	-156 ± 13	-395 ± 48	56	56	-7.11 ± 0.87	67	-
Amundsen Sea+		505 ± 24	-	232 ± 50	-156 ± 13	-484 ± 57	-	-	-	68	-
HH'	ABB*	28 ± 7	33 ± 9	4 ± 1	-29 ± 19	-86 ± 22	32	40	-2.72 ± 0.70	96	HE-thick
HH'	VEN*	13 ± 1	3 ± 1	8 ± 2	-8 ± 1	-15 ± 3	3	3	-4.82 ± 0.95	64	IPR
H'I	GEO*	88 ± 9	44 ± 12	17 ± 4	-28 ± 38	-144 ± 42	50	84	-2.88 ± 0.83	90	IPR
II'	WOR	12 ± 1	1 ± 0	2 ± 3	-	-10 ± 4	1	1	-14.79 ± 5.26	82	IPR
HI' Upscaling		35 ± 4	-	10 ± 2	-	-25 ± 6	-	-	-	72	-
Bellingshausen Sea		139 ± 11	82 ± 16	31 ± 10	-65 ± 43	-255 ± 22	86	128	-2.98 ± 0.26	89	-
Bellingshausen Sea+		174 ± 12	-	41 ± 13	-65 ± 43	-281 ± 23	-	-	-	87	-
I'I"	LBC	16 ± 2	27 ± 8	25 ± 3	-	-18 ± 8	60	60	-0.30 ± 0.14	42	IPR
JK	FRIS	230 ± 31	70 ± 20	250 ± 16	-	-50 ± 40	423	481	-0.12 ± 0.09	17	IPR
KK'	BRL	48 ± 12	24 ± 7	46 ± 8	-	-26 ± 16	79	80	-0.33 ± 0.20	36	HE-thick
K'A	JF	40 ± 11	17 ± 5	34 ± 5	-	-24 ± 13	46	47	-0.52 ± 0.27	41	HE-thick
I'K' Upscaling		28 ± 3	-	16 ± 2	-	-13 ± 2	-	-	-	45	-
Weddell Sea		334 ± 35	139 ± 23	355 ± 31	-	-118 ± 52	608	668	-0.19 ± 0.09	25	-
Weddell Sea+		363 ± 35	-	371 ± 33	-	-131 ± 53	-	-	-	26	-
Total Surveyed		1,573 ± 56	444 ± 36	1,106 ± 141	-282 ± 50	-1,193 ± 163	1,481	1,596	-0.81 ± 0.11	52	IPR (68%)
Total Upscaling		476 ± 67	-	216 ± 33	-	-261 ± 34	74	151	-3.53 ± 0.47	55	-
Total Antarctica		2,049 ± 87	-	1,321 ± 144	-282 ± 50	-1,454 ± 174	1,555	1,746	-0.94 ± 0.11	52	-

Grounding line flux (GLF); surface mass balance (SMB); calving flux (CF); non-steady state mass change (dh/dt), basal mass balance (BMB); ice shelf area (Area); ice shelf area, including islands and ice rises (Area+); mean specific basal mass balance (SBMB); melt ratio (MR); and ice thickness method, either by ice penetrating radar (IPR) or surface elevation-derived thickness (HE-thick). Ocean sectors with a "+" signs indicate that regional upscaling is included. Ice shelves with an asterisk indicate those that have been corrected for imbalance using ICESat elevation rates. Uncertainties are one standard deviation. See Supplementary Figure 1 for ice shelf names.

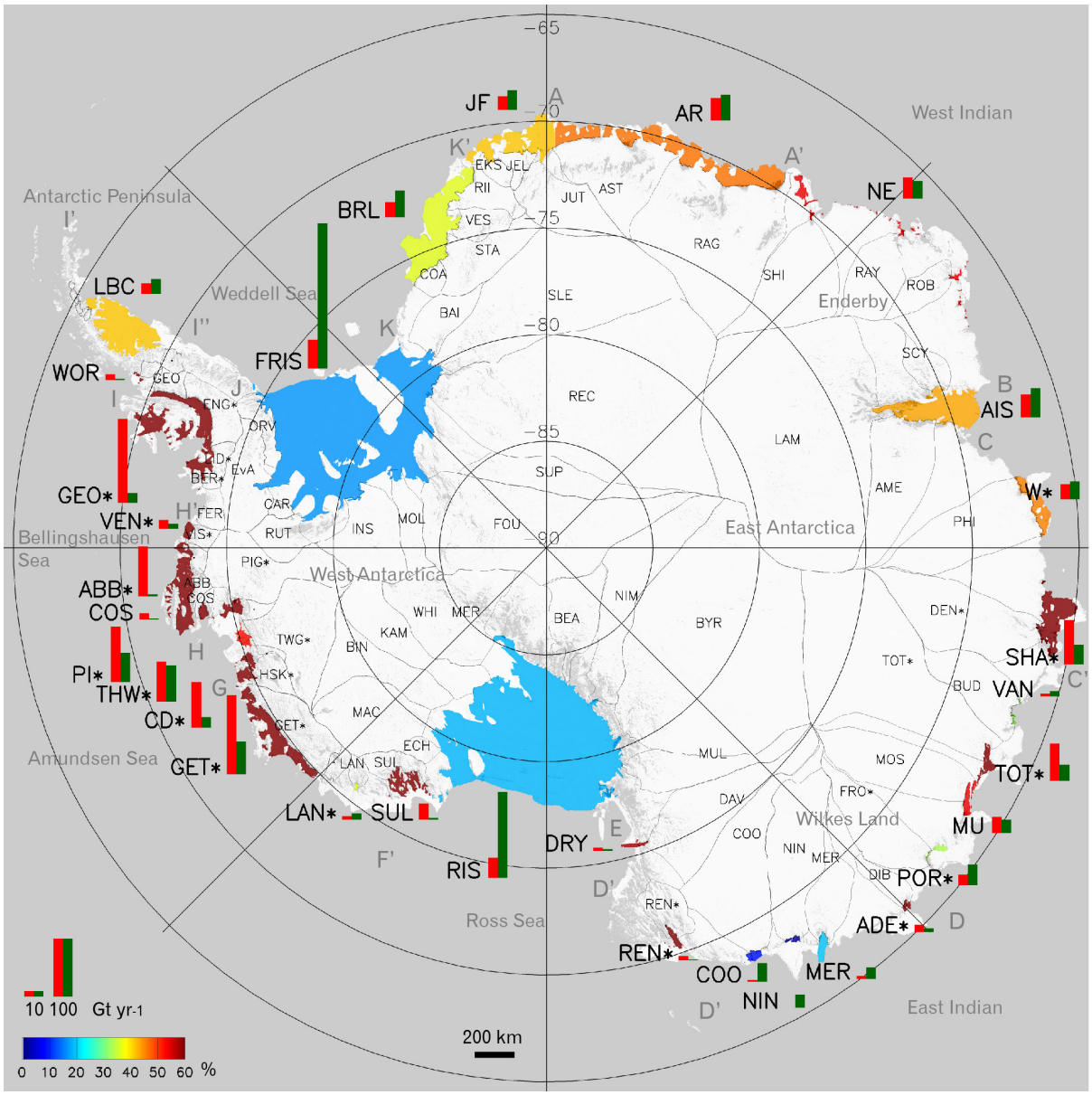

Supplementary Figure 1 Melt ratio of Antarctic ice shelves.
Ice shelves are colour-coded from blue to red for basal mass loss ratio (in % of total outflux). Red and green bars indicate fresh water fluxes from basal mass loss and icebergs calving, respectively (in Gt yr^{-1}). Bold black label indicate ice shelf names: Astrid-Ragnhild (AR), North-East (NE), Amery (AIS), West (W), Shackleton (SHA), Vanderford (VAN), Totten (TOT), Moscow University (MU), Porpoise (POR), Adélie (ADE), Mertz (MER), Ninnis (NIN), Cook (COO), Rennick (REN), Drygalski (DRY), Ross (RIS), Sulzberger (SUL), Land (LAN), Getz (GET), Crosson and Dotson (CD), Thwaites (THW), Pine Island (PI), Cosgrove (COS), Abbot (ABB), Venable (VEN), George VI (GEO), Wordie (WOR), Larsen B-C (LBC), Filchner-Ronne (FRIS), Brunt and Riiser-Larsen (BRL), and Jelbart and Fimbul (JF). Thin black lines and label indicate the drainage basins feeding ice shelves[58]. Asterisks indicate basins experiencing dynamic thinning[9] and ice shelves experiencing thinning[8]. Grey labels indicate oceanic sectors and major basins.

Supplementary Table 2 Basal mass balance (BMB) and mean specific basal mass balance (SBMB) comparison.

	This study			Timmermann et al., 2012		
Name	**Area**	**BMB**	**SBMB**	**Area**	**BMB**	**SBMB**
	10^3 km^2	Gt yr^{-1}	m yr^{-1}	10^3 km^2	Gt yr^{-1}	m yr^{-1}
FRIS	423	-50 ± 40	-0.12 ± 0.09	438	-138	-0.32
BRL	79	-26 ± 16	-0.33 ± 0.20	77	-65	-0.84
JF	46	-24 ± 13	-0.52 ± 0.27	53	-130	-2.45
LBC	60	-18 ± 8	-0.30 ± 0.14	52	-48	-0.92
GEO	50	-144 ± 16	-2.88 ± 0.32	27	-86	-3.19
ABB	32	-86 ± 11	-2.72 ± 0.36	33	-59	-1.82
PI	6	-95 ± 14	-15.96 ± 2.33	5	-13	-2.60
GET	33	-136 ± 19	-4.09 ± 0.58	35	-164	-4.69
RIS	477	-34 ± 25	-0.07 ± 0.05	475	-260	-0.55
AIS	60	-39 ± 21	-0.65 ± 0.35	67	-174	-2.60
Total	1266	-508 ± 64	-0.40 ± 0.05	1262	-1137	-0.90

Results from our study and from the ice-ocean modelling study of Timmermann et al.[18] are compared. Poor convergence of results is found for single and total numbers.

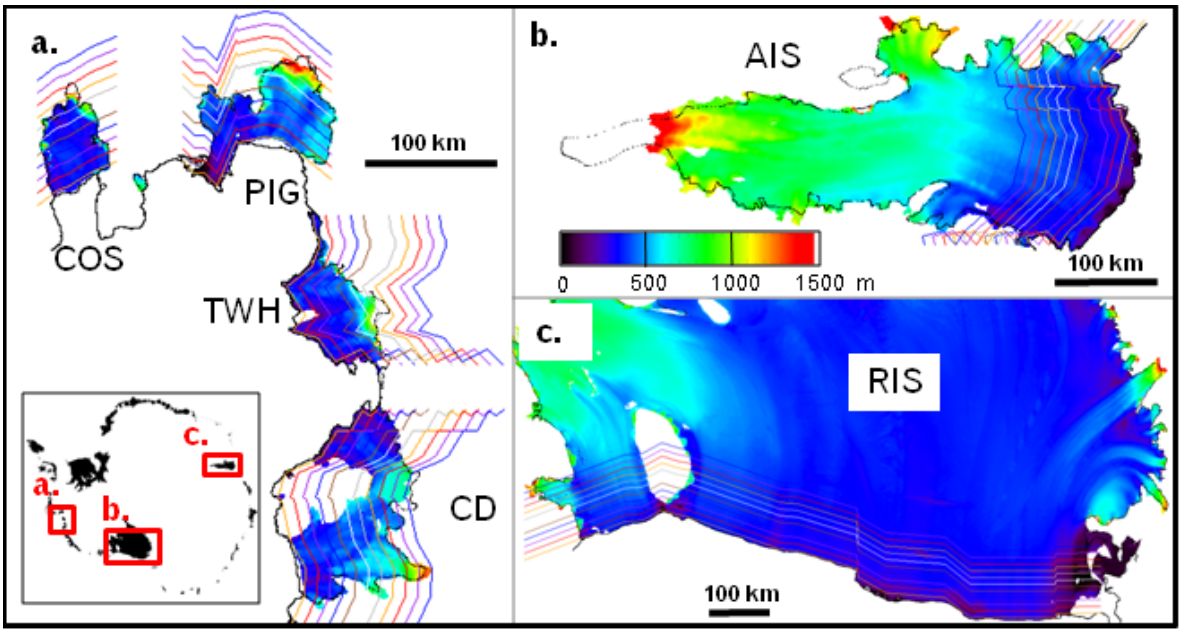

Supplementary Figure 2 Calving flux gates placement.
Ten calving flux gates were placed inland of our calving front gate with 10 km increments. Calving gates are plotted on top of ice-equivalent thickness. Thin black line for grounding lines and coastlines. See inset for localisation and Supplementary Figure 1 for ice shelves names.

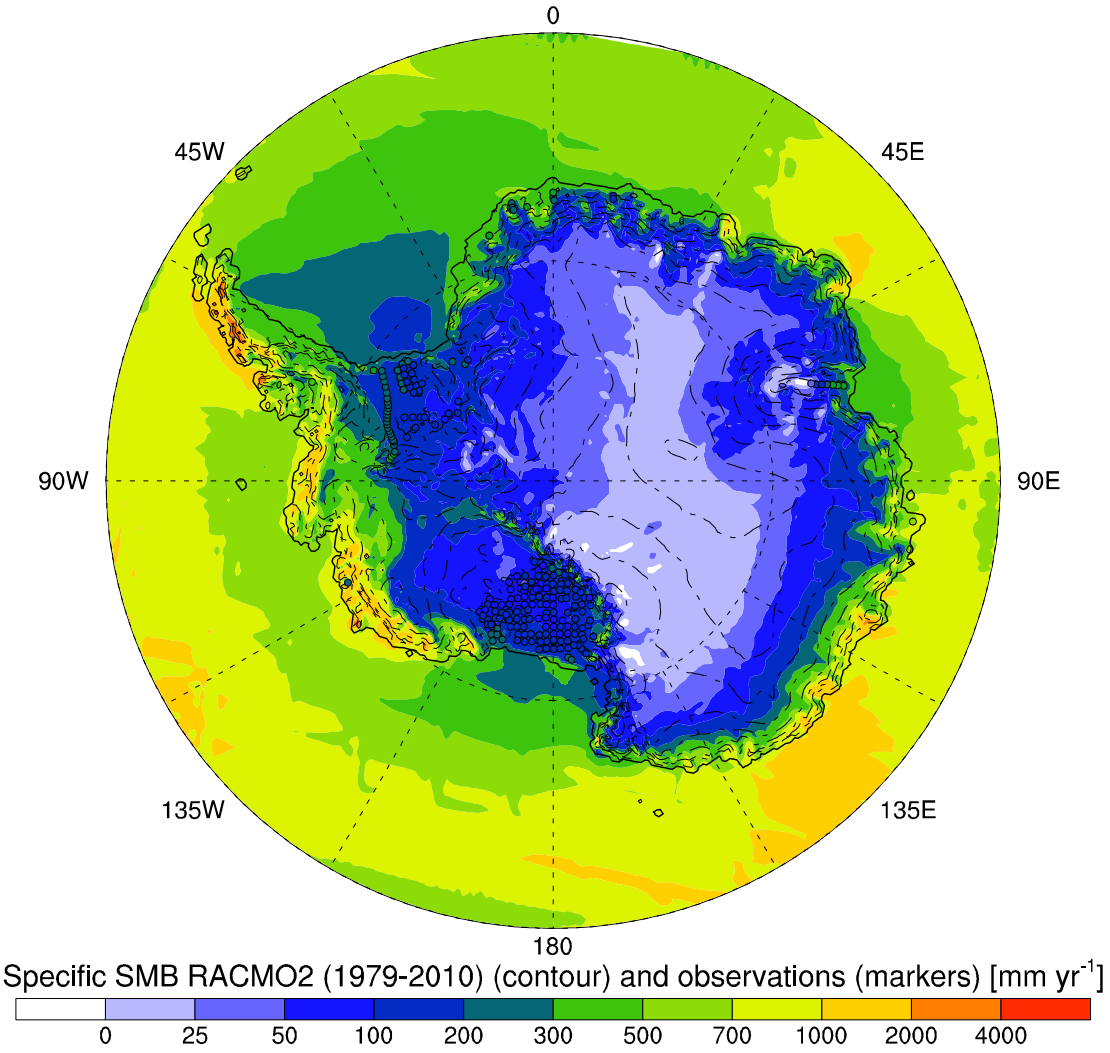

Supplementary Figure 3 Specific surface mass balance (average for years 1979–2010). Specific SMB simulated by RACMO2 (contours) and according to 315 observations on ice shelves (filled circles). Black line indicates the RACMO2 ice mask and dashed lines are elevation contours with 500 m increments. Note that on the seasonal sea-ice, specific SMB equals precipitation (P) minus surface sublimation (SU_s) and on open ocean SMB = P.

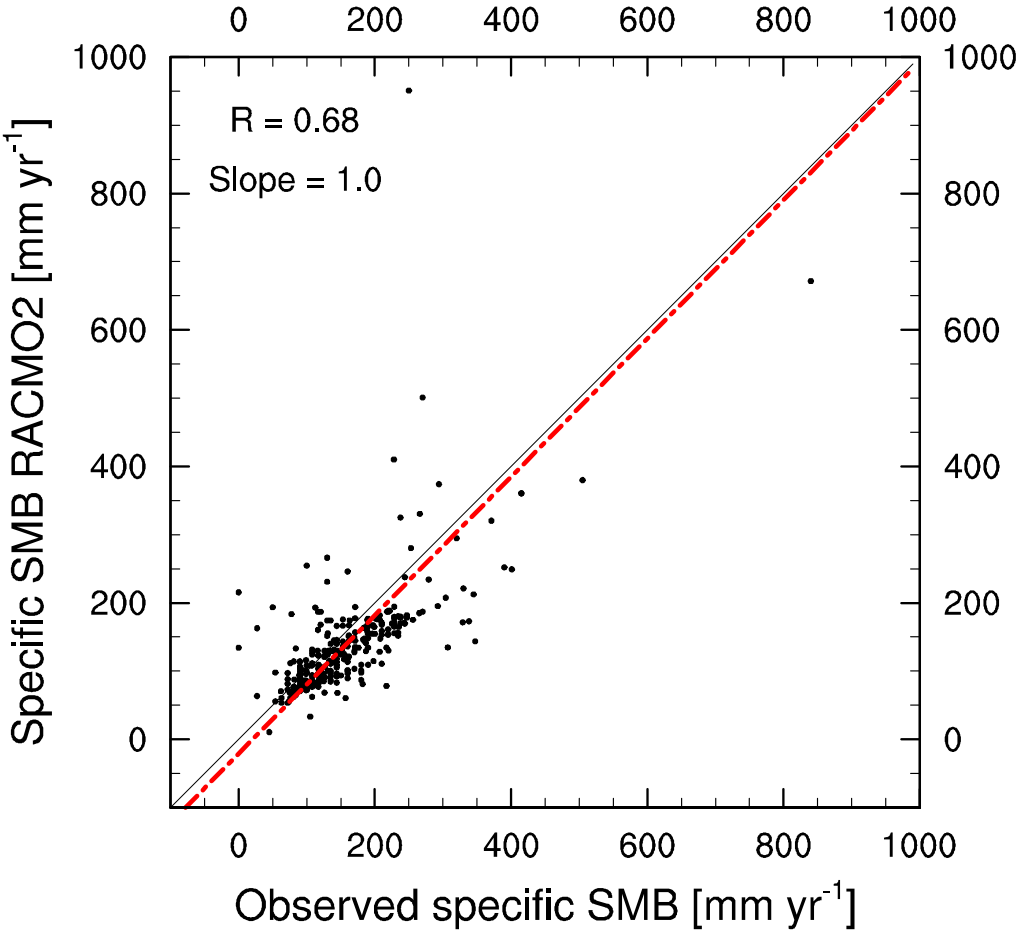

Supplementary Figure 4 Observed versus modelled specific SMB on Antarctic ice shelves. The black line represents the 1:1 line, and the red dashed line is least squares linear fit determined by the smallest perpendicular distance from each model value to the observational value. See Supplementary Figure 3 for location of the 315 observations.

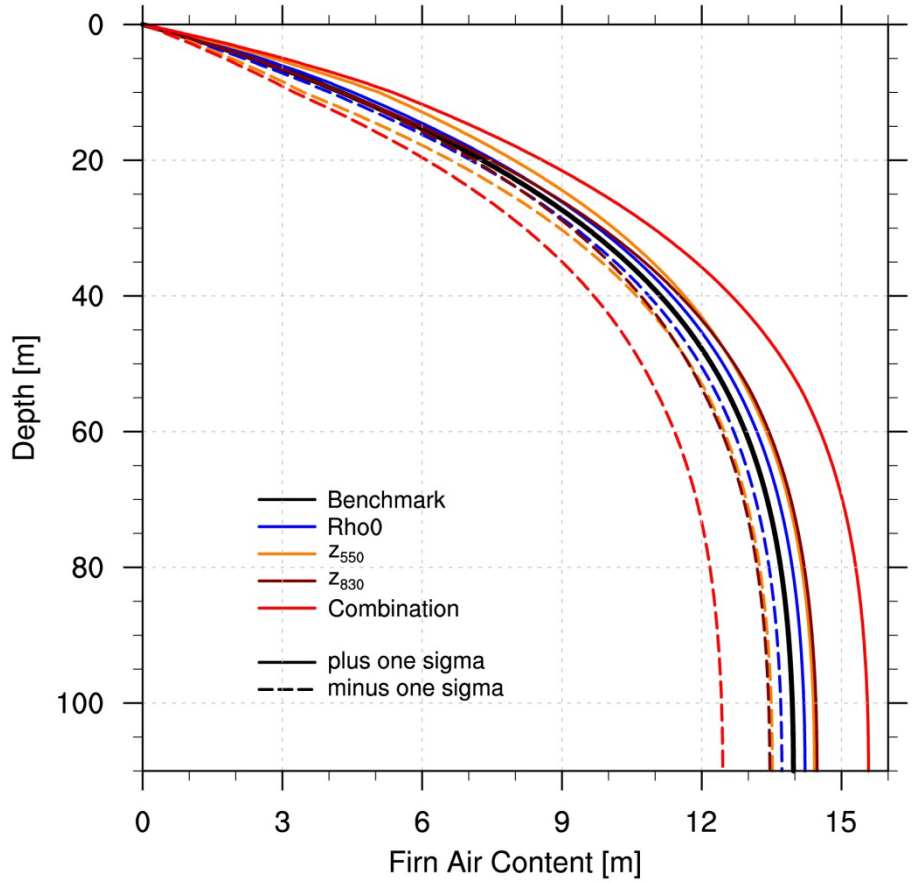

Supplementary Figure 5 Sensitivity runs for firn air content.
Vertically integrated firn air content for nine sensitivity runs with the firn densification model (FDM) for a point on the Ross ice shelf (82ºS, 172ºW); control simulation (black), including the uncertainty in surface density (Rho_0, blue), the 550 kg m^{-3} level (z_{550}, orange), the 830 kg m^{-3} level (z_{830}, brown) and with a combination of uncertainties (red). Positive (solid lines) and negative (dashed lines) one sigma ranges are shown.

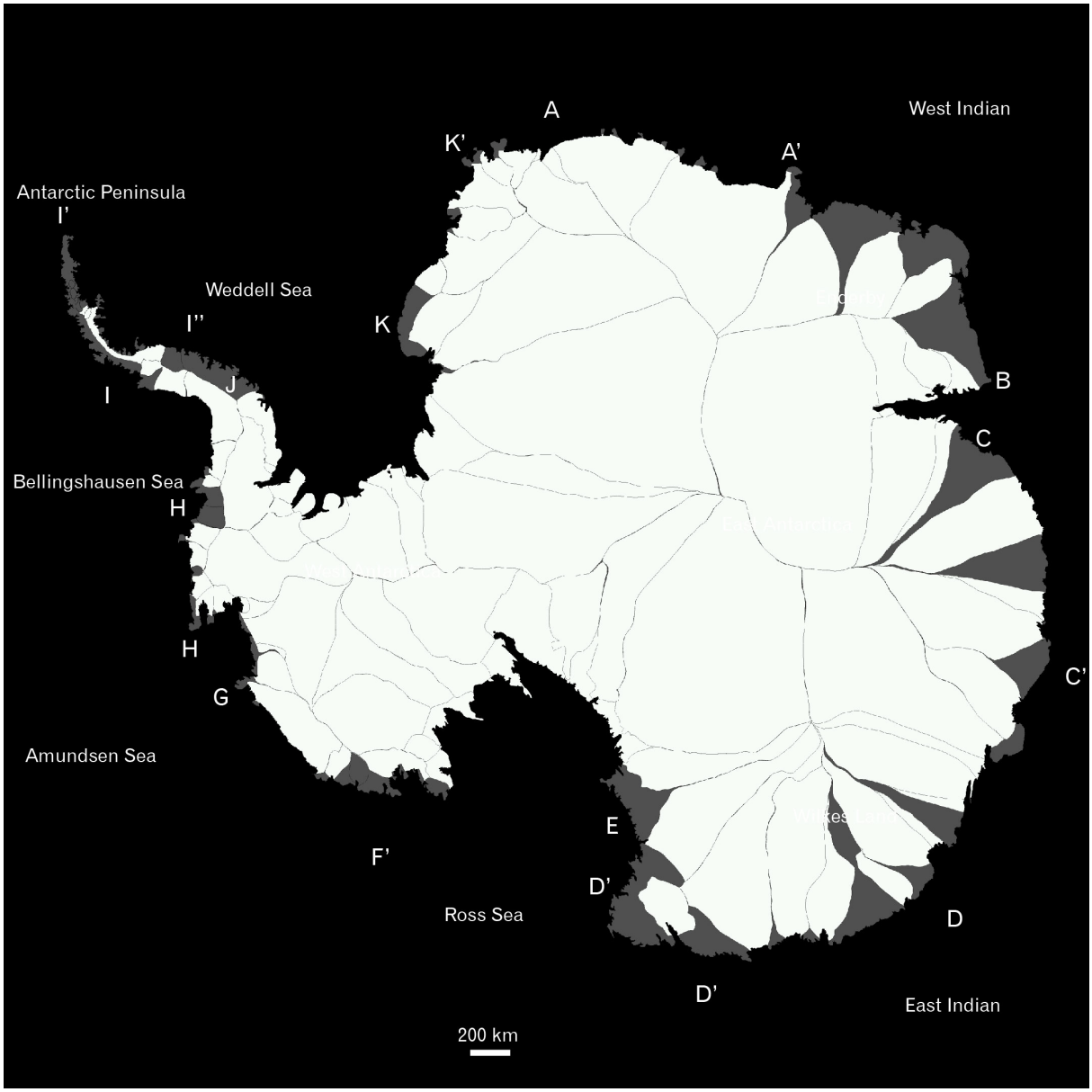

Supplementary Figure 6 Surveyed and un-surveyed areas.
The drainage basins surveyed by our calving/melting analysis (90% in area) are shown in white. The un-surveyed areas used in the upscaling (see Supplementary Discussion 3) are shown in grey.

Supplementary References

32 Tournadre, J., Girard-Ardhuin, F. & Legrésy, B. Antarctic icebergs distributions, 2002-2010. *J. Geophys. Res.* **117**, C05004, doi:10.1029/2011jc007441 (2012).

33 Gladstone, R. & Bigg, G. R. Satellite tracking of icebergs in the Weddell Sea. *Antarctic Sci.* **14**, 278-287, doi:10.1017/S0954102002000032 (2002).

34 Fretwell, P. *et al.* Bedmap2: improved ice bed, surface and thickness datasets for Antarctica. *Cryosphere* **7**, 375-393, doi:10.5194/tc-7-375-2013 (2013).

35 Rignot, E., Jacobs, S., Mouginot, J. & Scheuchl, B. Ice Shelf Melting Around Antarctica. *Science* (2013), doi:10.1126/science.1235798.

36 Bamber, J. L., Gomez-Dans, J. L. & Griggs, J. A. A new 1 km digital elevation model of the Antarctic derived from combined satellite radar and laser data - Part 1: Data and methods. *Cryosphere* **3**, 101-111 (2009).

37 Wen, J. *et al.* Basal melting and freezing under the Amery Ice Shelf, East Antarctica. *J. Glaciol.* **56**, 81-90 (2010).

38 Foldvik, A., Gammelsrød, T., Nygaard, E. & Østerhus, S. Current measurements near Ronne Ice Shelf: Implications for circulation and melting. *J. Geophys. Res.* **106**, 4463-4477, doi:10.1029/2000jc000217 (2001).

39 Gammelsrod, T. *et al.* in *The Polar Oceans and Their Role in Shaping the Global Environment* Vol. 85 *Geophys. Monogr. Ser.* 159-176 (AGU, 1994).

40 Scambos, T. A., Haran, T. M., Fahnestock, M. A., Painter, T. H. & Bohlander, J. MODIS-based Mosaic of Antarctica (MOA) data sets: Continent-wide surface morphology and snow grain size. *Remote Sens. Environ.* **111**, 242-257 (2007).

41 Bindschadler, R. *et al.* Getting around Antarctica: new high-resolution mappings of the grounded and freely-floating boundaries of the Antarctic ice sheet created for the International Polar Year. *Cryosphere* **5**, 569-588, doi:10.5194/tc-5-569-2011 (2011).

42 Fricker, H. A. & Padman, L. Ice shelf grounding zone structure from ICESat laser altimetry. *Geophys. Res. Lett.* **33**, doi:10.1029/2006gl026907 (2006).

43 Rignot, E., Mouginot, J. & Scheuchl, B. Antarctic grounding line mapping from differential satellite radar interferometry. *Geophys. Res. Lett.* **38**, L10504, doi:10.1029/2011gl047109 (2011).

44 Brunt, K. M., Fricker, H. A., Padman, L., Scambos, T. A. & O'Neel, S. Mapping the grounding zone of the Ross Ice Shelf, Antarctica, using ICESat laser altimetry. *Ann. Glaciol.* **51**, 71-79 (2010).

45 Brunt, K. M., Fricker, H. A. & Padman, L. Analysis of ice plains of the FilchnerRonne Ice Shelf, Antarctica, using ICESat laser altimetry. *J. Glaciol.* **57**, 965-975 (2011).

46 Joughin, I., Smith, B. E. & Holland, D. M. Sensitivity of 21st century sea level to ocean-induced thinning of Pine Island Glacier, Antarctica. *Geophys. Res. Lett.* **37**, L20502, doi:10.1029/2010gl044819 (2010).

47 Tinto, K. J. & Bell, R. E. Progressive unpinning of Thwaites Glacier from newly identified offshore ridge: Constraints from aerogravity. *Geophys. Res. Lett.* **38**, n/a-n/a, doi:10.1029/2011gl049026 (2011).

48 Rignot, E. Evidence for rapid retreat and mass loss of Thwaites Glacier, West Antarctica. *J. Glaciol.* **47**, 213-222 (2001).

49 Rignot, E. Changes in West Antarctic ice stream dynamics observed with ALOS PALSAR data. *Geophys. Res. Lett.* **35**, doi:10.1029/2008gl033365 (2008).

50 Fricker, H. A. *et al.* Mapping the grounding zone of the Amery Ice Shelf, East Antarctica using InSAR, MODIS and ICESat. *Antarctic Sci.* **21**, 515-532, doi:10.1017/s095410200999023x (2009).

51 Galton-Fenzi, B. K., Hunter, J. R., Coleman, R. & Young, N. A decade of change in the hydraulic connection between an Antarctic epishelf lake and the ocean. *J. Glaciol.* **58**, 223-228, doi:10.3189/2012JoG10J206 (2012).

52 Sykes, H. J., Murray, T. & Luckman, A. The location of the grounding zone of Evans Ice Stream, Antarctica, investigated using SAR interferometry and modelling. *Ann. Glaciol.* **50**, 35-40, doi:10.3189/172756409789624292 (2009).
53 Jansen, D. *et al.* Present stability of the Larsen C ice shelf, Antarctic Peninsula*J. Glaciol.* **56**, 593-600, doi:10.3189/002214310793146223 (2010).
54 Jezek, K., and RAMP Product Team (ed AK: Alaska SAR Facility in association with the National Snow and Ice Data Center Fairbanks) (CO. Digital media, Boulder 2002).
55 Bindschadler, R. *et al.* The Landsat Image Mosaic of Antarctica. *Remote Sens. Environ.* **112**, 4214-4226 (2008).
56 Orheim, O. Evolution of under-water sides of ice shelves and icebergs *Ann. Glaciol.* **9**, 176-182 (1987).
57 van de Berg, W. J., van den Broeke, M. R., Reijmer, C. H. & van Meijgaard, E. Reassessment of the Antarctic surface mass balance using calibrated output of a regional atmospheric climate model. *J. Geophys. Res.* **111**, D11104, doi:10.1029/2005jd006495 (2006).
58 Rignot, E. *et al.* Recent Antarctic ice mass loss from radar interferometry and regional climate modelling. *Nature Geosci.* **1**, 106-110, doi:10.1038/ngeo102 (2008).
59 Kaspers, K. A. *et al.* Model calculations of the age of firn air across the Antarctic continent. *Atmos. Chem. Phys.* **4**, 1365-1380, doi:10.5194/acp-4-1365-2004 (2004).
60 van den Broeke, M. Depth and Density of the Antarctic Firn Layer. *Arct. Antarct. Alp. Res.* **40**, 432-438 (2008).